Chains of magnetite crystals in the meteorite ALH84001: Evidence of biological origin

E. Imre Friedmann*†‡, Jacek Wierzchos§, Carmen Ascaso¶, and Michael Winklhofer‖

*Department of Biological Science, Florida State University, Tallahassee, FL 32306-1100; †Space Science Division 245-3, National Aeronautics and Space Administration Ames Research Center, Moffett Field, CA 94035; §Servei de Microscòpia Electrònica, Universitat de Lleida, 25196 Lleida, Spain; ¶Centro de Ciencias Medioambientales, Consejo Superior de Investigaciones Científicas, 28006 Madrid, Spain; and ‖Institut für Geophysik, Universität München, D-80333 Munich, Germany

Edited by Rita R. Colwell, National Science Foundation, Arlington, VA, and approved January 10, 2001 (received for review October 27, 2000)

The presence of magnetite crystal chains, considered missing evidence for the biological origin of magnetite in ALH84001 [Thomas-Keprta, K. L., Bazylinski, D. A., Kirschvink, J. L., Clemett, S. J., McKay, D. S., Wentworth, S. J., Vali, H., Gibson, E. K., Jr., & Romanek, C. S. (2000) *Geochim. Cosmochim. Acta* 64, 4049–4081], is demonstrated by high-power stereo backscattered scanning electron microscopy. Five characteristics of such chains (uniform crystal size and shape within chains, gaps between crystals, orientation of elongated crystals along the chain axis, flexibility of chains, and a halo that is a possible remnant of a membrane around chains), observed or inferred to be present in magnetotactic bacteria but incompatible with a nonbiological origin, are shown to be present. Although it is unlikely that magnetotactic bacteria were ever alive in ALH84001, decomposed remains of such organisms could have been deposited in cracks in the rock while it was still on the surface on Mars.

In 1996, McKay *et al.* (1) suggested that the Martian meteorite ALH84001 harbors relics of early biological activity. Thomas-Keprta *et al.* (2) proposed that magnetite crystals in the meteorite are magnetofossils and postulated six criteria that characterize biologically produced magnetite crystals. The simultaneous presence of all six characteristics—i.e., a definite size range and width/length ratio, chemical purity, crystallographic perfection, arrangement of crystals in linear chains, unusual crystal morphology, and elongation of crystals in the [111] crystallographic direction—should constitute evidence of biological origin. These researchers demonstrated the presence of five of these characteristics but not of the sixth—i.e., magnetite crystals in linear chains—because the method used, dissolution of the carbonate in 20% acetic acid, causes the chains to collapse. Earlier, we reported magnetite chains in ALH84011 (3), and here we present more complete information. We used high-power backscattered scanning electron microscopy (SEM-BSE), a method introduced by two of us (J.W. and C.A.) to study endolithic microorganisms (e.g., see ref. 4). Whereas in conventional SEM (SEM-SE) images of surface structures are formed by reflected secondary electrons, SEM-BSE uses backscattered electrons that originate from below the surface, in our material from a depth of up to about 400-1000 nm, as determined by Monte Carlo trajectory simulation (5). SEM-BSE records not surface morphologies but chemical compositions, as structures composed of heavier elements appear brighter than those of lighter ones. Resolution is limited by the scattered nature of the signal, so images of very small objects appear fuzzy. Also, chains oriented obliquely to the image plane may not be resolved. To alleviate these problems, we used here SEM-BSE in the three-dimensional (stereo) mode. Our method thus made possible the *in situ* direct visualization of the spatial arrangement of nanometer-sized structures inside the rock substrate.

Magnetotactic Bacteria and Magnetosomes. Terrestrial magnetotactic bacteria form magnetosomes, single-domain crystals of magnetite (Fe_3O_4) or greigite (Fe_3S_4) surrounded by a biological membrane. The magnetosomes are arranged in linear chains, held together by organic material, which fills the narrow gaps between them (6, 7). Because of the elastic property of this material, the chains have a remarkable elastic stability (8). In the chains, the crystals are roughly cuboidal, elongated, or bullet-shaped, and the crystal morphology is characteristic of the species or strain. The size of crystals generally falls within the theoretical limits of single-domain grain size (9). Magnetotactic bacteria live mostly at the water-sediment interface in both marine and freshwater habitats, where microaerobic conditions are frequently present. The bacteria function as permanent magnetic dipoles and are passively aligned, like a compass, along the prevailing magnetic field lines (7). All magnetotactic bacteria are motile (10). Magnetotaxis appears to be advantageous for finding and maintaining an optimal position along a vertical O_2 concentration gradient in an oxic/anoxic transition zone, characteristic of microaerobic environments (7, 11).

Magnetite Chains as Indicators of Biological Origin. The formation of magnetite crystals within a definite size range and their arrangement in linear chains is in itself a conspicuous example of genetically controlled biomineralization (7, 12). Magnetosome chains are not in the energetically most favorable configuration, as the total energy of the system can be reduced if the particles are allowed to collapse into a clump (13) or into a jackknife structure (14). No inorganic process is known to produce similar structures. Below we suggest five additional morphological characteristics that are present in biologically formed magnetite chains. The first four of these criteria, listed below, are evident from the numerous published transmission electron micrographs of various magnetotactic bacteria (e.g., in refs. 6, 7, 10, 11, 15, and 16), which show consistent morphological characteristics, whereas the fifth is based on observations (8) on postmortem changes in magnetosome chains in bacteria. Such magnetite chains could not be formed abiotically—e.g., in a strong magnetic field, by crystals concentrated at grain boundaries, or by being accidentally positioned into a narrow channel in the rock substrate.

(*i*) *Uniform crystal size and shape within chains*. Despite the considerable range of variation in magnetite crystal size and shape (isodiametric or elongated) within a bacterial species (2), the crystals within individual chains are of similar size because each is formed at the end of the chain as it grows into a preformed membrane vesicle, which appears to function as a template. (*ii*) *Gaps between crystals.* Crystals in chains are separated by gaps ascribable to the membrane bounding the magnetosomes and to the organic substance between them, as seen in *Magnetospirillum magnetotacticum* (Fig. 1*C*). Magnetite

This paper was submitted directly (Track II) to the PNAS office.

Abbreviations: SEM-BSE, scanning electron microscopy in backscattered electron mode; SEM-SE, electron microscopy in secondary electron mode; LEDS, low-electron-density substance.

‡To whom reprint requests should be sent at the † address, the present address: E-mail: friedmann@bio.fsu.edu or friedmann@gal.arc.nasa.gov.

 www.pnas.org/cgi/doi/10.1073/pnas.051514698

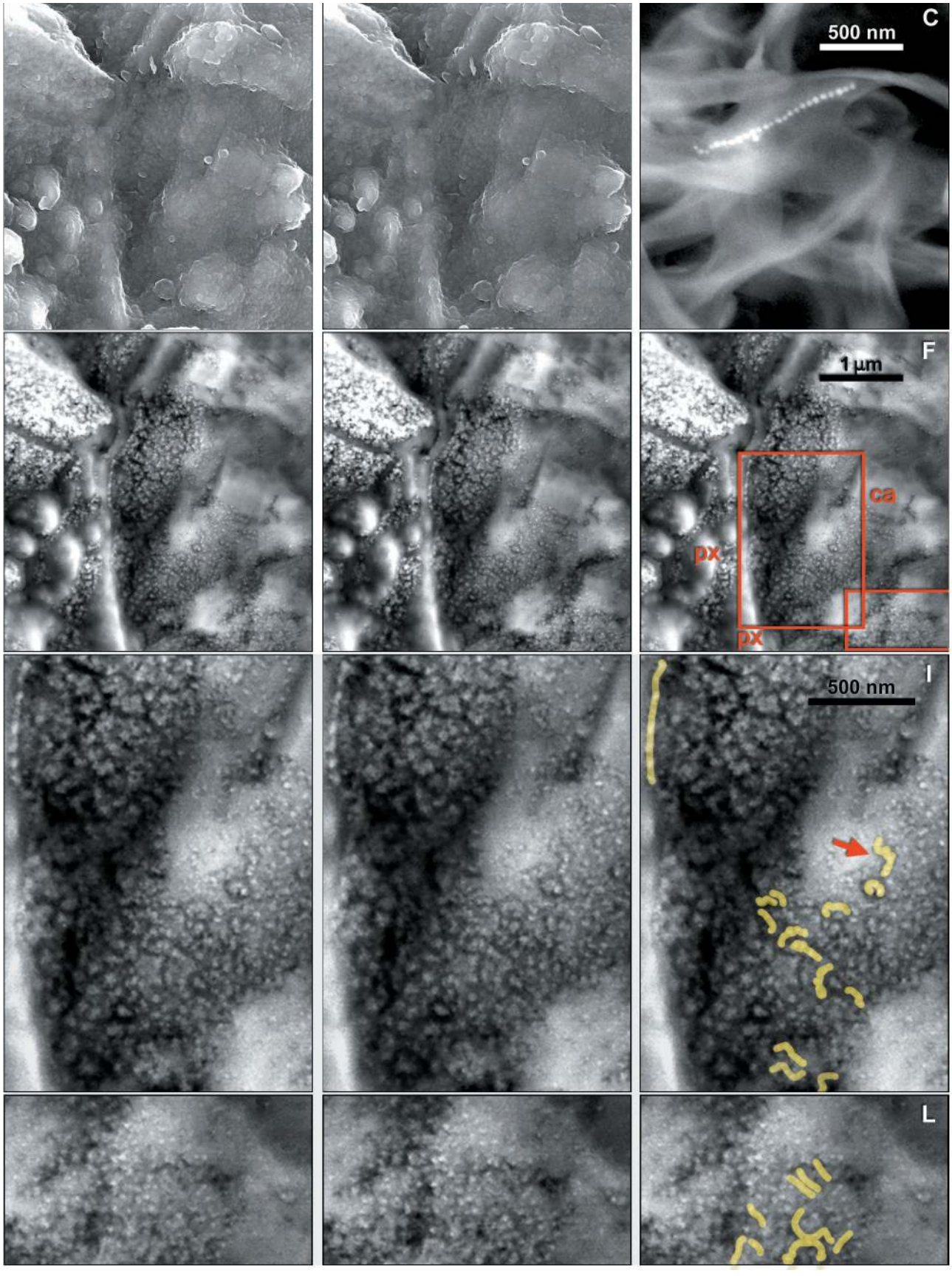

Fig. 1. (*A* and *B*) SEM-SE stereo micrograph of area in Fig. 4*A*, showing surface features. (*C*) SEM-BSE image of magnetosome chain in freeze-dried culture of *Magnetospirillum magnetotacticum.* (*D* and *E*) SEM-BSE stereo micrograph of *A* and *B.* (*F*) Outlines of areas shown in *G* and *H* and *J* and *K*. (*I* and *L*) Chains visible in *G* and *H* and *J* and *K*, respectively, are highlighted. px, orthopyroxene; ca, carbonate.

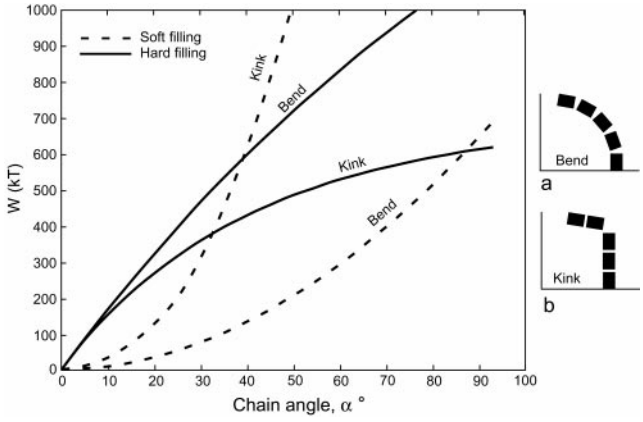

Fig. 2. Total energy [$W(kT)$], in units of thermal energy kT of a magnetite crystal chain plotted against the angle between the first and last particle of the chain, as calculated according to Eq. **8** in *Appendix 1,* which is published as supplementary material on the PNAS web site, www.pnas.org. For the case of soft gap fillings, the total energy is the sum of magnetic energy (Eq. **8**) and elastic energy (Eq. **10**). The energetically preferred deformation mode (lower value of W) is bending (*a*) for soft gap fillings and kink formation (*b*) for rigid gap fillings. Number of particles in chain $n = 5$; particle size $a = 50$ nm; length/width ratio = 1.4; gap space $qa = 10$ nm; Young modulus of soft material $E = 0.1$ MPa (10^6 dyn·cm^{-2}). $kT = 4 \times 10^{-14}$ J.

crystal chains formed nonbiologically (e.g., in a strong magnetic field) would abut without gaps. (*iii*) *Orientation of elongated crystals.* In chains of elongated magnetosomes the crystals are oriented with the long axes along the chain. The energetically more favorable arrangement would be a side-by-side position (i.e., with their long axes perpendicular to the chain axis) where every second particle has opposite magnetization as in a multidomain state, so as to reduce the magnetic stray field of the configuration. (*iv*) *Halo (traces of membrane) around chains*. At the magnifications used, the traces of membranes surrounding magnetosomes (6) should be detectable as thin halos around fossil chains. (*v*) *Flexibility of chains*. Magnetosome chains do not necessarily disintegrate upon death of the bacterium but may undergo strong but smooth bends (8) and become fossilized in that position (14). Mathematical analysis (8) has revealed that it is the elastic property of the soft organic material between the crystals (and not crystal morphology) that imparts stability and flexibility to such chains, resulting in deformations into smooth arcs (Fig. 2*a*). A chain with rigid gap filling will respond with a sharp kink in the middle of the chain (Fig. 2*b*), so that the whole elastic transformation is concentrated in a single gap rather than being equally distributed over all gaps. In Fig. 2, the total energy (W) of a magnetosome chain is plotted against the angle between the first and last magnetosome in the chain for soft and rigid gap fillings and for bend and kink modes of deformation. The energetically preferred deformation mode (lower value of W) is bending for soft gap filling but formation of a sharp kink for rigid gap filling. [Derivation of the $W(\alpha)$ curves and further details are given in *Appendix 1,* which is published as supplemental data on the PNAS web site, www.pnas.org.] Significantly, all soft and elastic, yet electron-transparent (low-atomic-number), substances are of biological origin, and no inorganic (mineral), naturally occurring substance is known to have such properties.

Materials and Methods

We examined fragments of rock chip ,270 (parent ,221) from the meteorite ALH84001. Specimens were either embedded in resin, cut with a diamond saw, ground, polished, and coated with 10 nm of carbon or fractured and coated without embedding. For SEM-BSE and SEM-SE imaging the following microscopes were used: tungsten-filament Zeiss DSM940A (Fig. 3 *A, D,* and *E*), field emission Zeiss Gemini 982 (Fig. 3 *B*, *C*, and *F* and Fig. 4*C*), Philips EFEGXL20 (Fig. 1*C*), and LEO 1525 (Fig. 1 *A, B,* and *D–L* and Fig. 4 *A* and *B*). The fuzziness of images was reduced by an analySIS (Soft Imaging System, Münster, Germany) DCE (differential contrast enhancement) filter. Energy-dispersive x-ray spectroscopy microanalysis was performed with a Link ISIS Oxford and a Kevex 8000 Quantum system and for Fig. 4*B* with an IXRF system. Auger electron spectroscopy was done in a PHI model 670 scanning Auger microscope (Physical Electronics, Eden Prairie, MN) equipped with a Schottky FE electron gun. Stereo micrograph pairs were tilted at 7°.

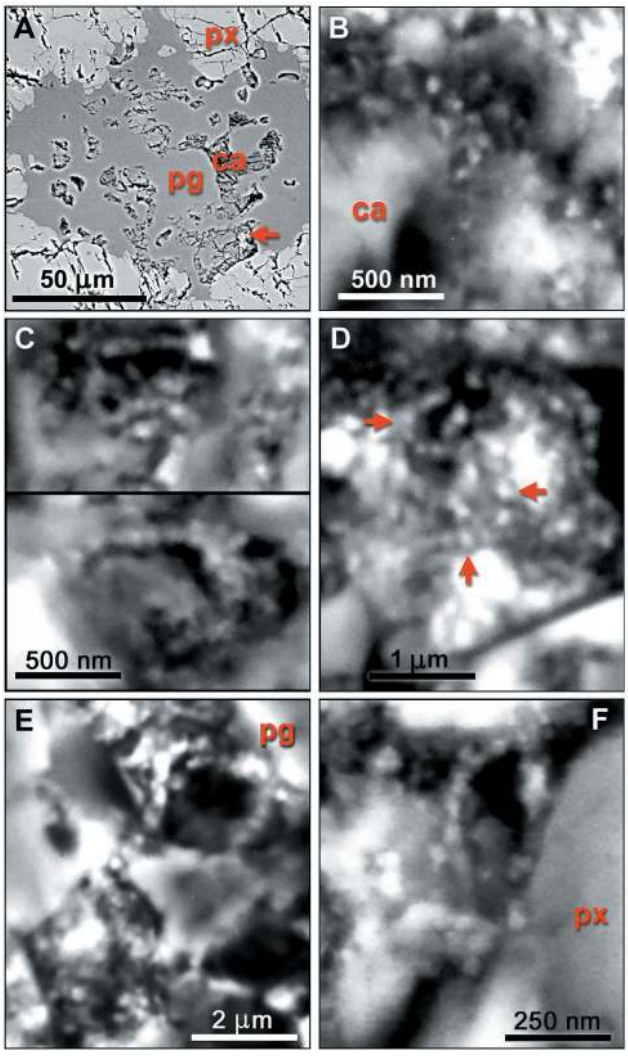

Fig. 3. SEM-BSE micrographs of resin-embedded and polished specimens of rim regions of carbonate globules. (*A*) Lobes of a carbonate globule (ca) surrounded by plagioclase glass (pg) and orthopyroxene (px); arrow: site of *E*. (*B*) Magnetite chain with uniform gaps between particles. (*C–E*) Magnetite chains with strong bends; the S-shaped structure in *D* (arrows) may be composed from two chains. (*F*) Chain of elongated particles aligned along their long axes.

Results

Magnetite Crystals and Chains. The typical setting of magnetite crystals in the rim region of a carbonate globule is shown in Fig. 4 *A* and *B*. This specimen was fractured and carbon coated without resin embedding, and imaging was through the intact surface. The wide iron-rich rim stretches approximately vertically,

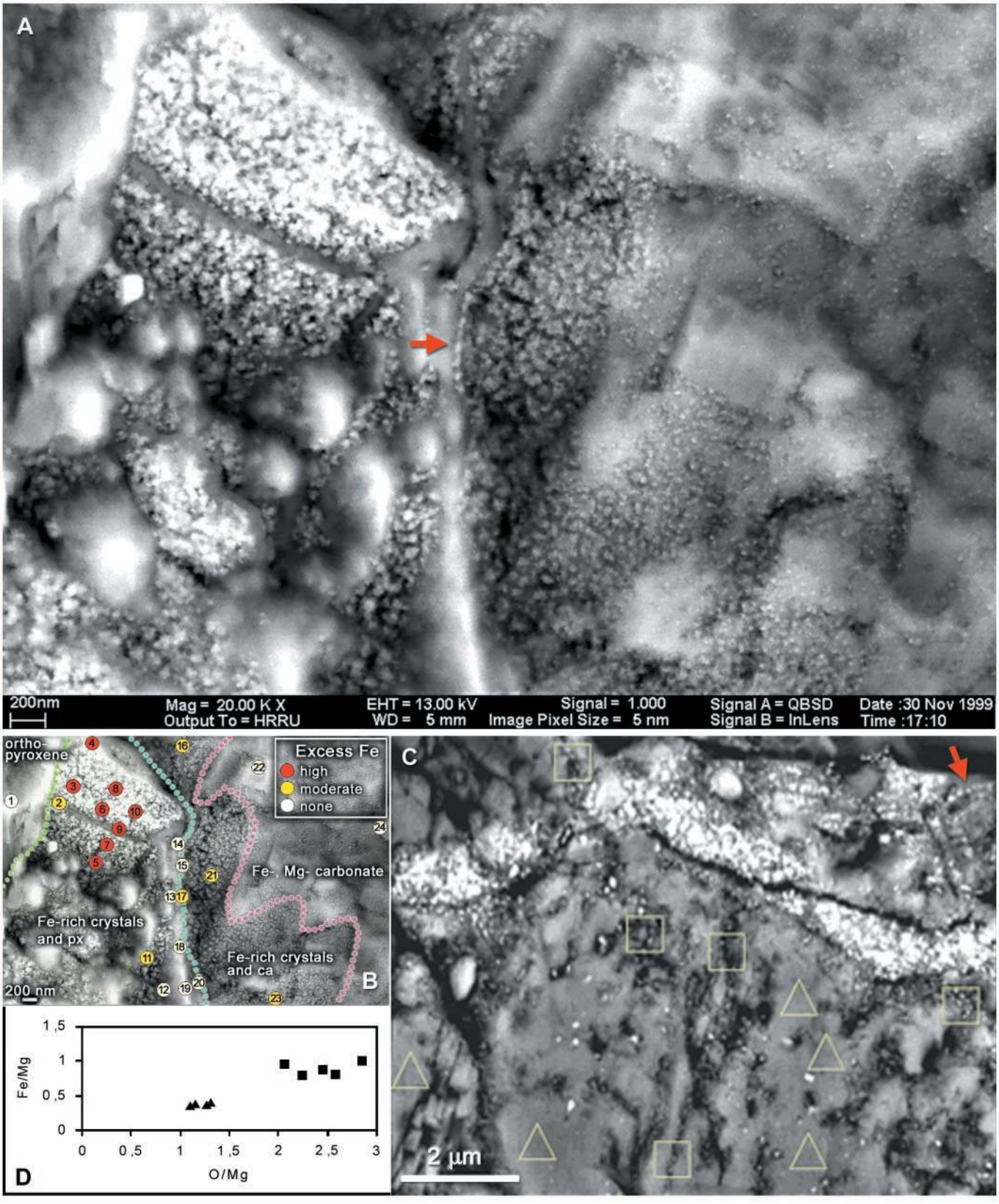

Fig. 4. (*A–C*) SEM-BSE micrographs of magnetite crystals in the rim region of carbonate globules in ALH84001. (*A*) Imaged through the intact surface of a freshly fractured specimen, chain of large elongated crystals (arrow), further chains of smaller crystals and other details in Fig. 1. (*B*) Energy-dispersive x-ray spectrometry analyses of elemental composition showing position of Fe-rich rim (detailed data are presented in *Appendix 2,* which is published as supplemental data on the PNAS web site, www.pnas.org). (*C*) Similar site in a resin-embedded, sectioned, and polished specimen, one chain marked by arrow, also site of Auger electron spectroscopy analyses. (*D*) Results of analyses of areas outlined in *C*: squares, magnetite crystal chains present; triangles, absent; ca, carbonate; px, orthopyroxene.

Table 1. Frequency distribution of number of magnetite crystals in chains

No. of crystals	No. of chains
4	41
5	32
6	27
7	24
8	13
9	6
10	5
11	3
12	2
13	1

evident as a zone of small granules overlying the substrate, orthopyroxene between green and blue lines and carbonate between blue and purple (Fig. 4*B*). Elemental analysis (below) indicates that the granules are rich in Fe and O, with only traces of S. Previous studies (1, 2) showed that these Fe- and O-rich rims are composed mainly of magnetite crystals, with a few grains possibly of iron sulfides, embedded in carbonate matrix. The stereo pair in Fig. 1 *A* and *B* shows the surface of the area in SEM-SE, whereas Fig. 1 *D* and *E*, in SEM-BSE, shows the underlying structures up to *ca.* 1 μm deep. Comparison of these images reveals that the entire area is covered by a low-electron-density (i.e., low-atomic-number) substance (LEDS) of unknown (perhaps organic?) chemical composition, with a granular surface visible in SEM-SE but transparent in the BSE mode. Fig. 1*C* is an SEM-BSE image of a magnetosome chain in a freeze-dried preparation of *Magnetospirillum magnetotacticum*, shown for comparison. The areas indicated in Fig. 1*F* are shown in BSE stereo pairs in Fig. 1 *G* and *H* and Fig. 1 *J* and *K*. In these stereo images the magnetite crystals embedded in transparent LEDS appear as though floating, whereas others are embedded in the large carbonate crystals. In the large crystal conglomeration in the upper left corner of Fig. 4*A*, the individual crystals are not resolved, because of superposition of the BSE signals. In other, less compacted clusters, individual crystals are distinguishable, and among these, many appear to form chains. In Fig. 4*A* a conspicuous chain of 7 or 8 elongated crystals arranged along their long axes is indicated by an arrow. In the stereo image pairs in Fig. 1 *G* and *H* and Fig. 1 *J* and *K*, several chains of various lengths, clarity, and state of imaging can be distinguished, as indicated in the auxiliary Fig. 1 *I* and *L*. The SEM-BSE micrographs in Fig. 3 *A–F* and Fig. 4*C* are of resin-embedded specimens. In the sectioned specimen shown in Fig. 3*A* the small carbonate structures (probably lobes of a carbonate globule) are embedded in plagioclase glass and orthopyroxene. The arrow indicates the site of the chain shown in Fig. 3*E*. Fig. 3*B* is a chain of six crystals clearly separated by gaps. Fig. 3 *C* and *D* show crystal chains with strong bends; in Fig. 3*D* the apparent S-shaped structure (arrows) may be composed of two chains. The bent chain of about 15 large isodiametric crystals in Fig. 3*E* and the chain of 6 small elongated crystals arranged in the direction of their long axes in Fig. 3*F* illustrate the wide range of crystal forms and sizes in ALH84001 (note different scales). Significantly, the size and shape of crystals within each chain are uniform. Many or perhaps most magnetite crystals, both single and in chains, seem to be surrounded, at least in part, by LEDS, which appears in SEM-BSE as a dark area. Because such areas are evident both in unprocessed (i.e., freshly fractured, Fig. 4*A*) and in resin-embedded (Figs. 3 *B–F* and 4*C*) specimens, they are not voids but filled with LEDS. A chain in Fig. 1 *G* and *H* (marked by an arrow in Fig. 1*I*) is surrounded by a dark halo, evident against the white background of carbonate in which the chain is embedded. Similar halos, if present around other chains, may not be visible against the dark LEDS background. Fig. 4*C* is a resin-embedded specimen with numerous chains and chain fragments. One chain is marked by an arrow, others are inside squares. The chain in the rightmost square is shown in Fig. 3*B*.

The number of magnetite crystals in the chains varied greatly. The frequency distribution of 154 magnetite chains consisting of at least four crystals (Table 1) shows a non-Gaussian pattern, which suggests that the chains are not representative of a natural population but probably are disrupted fragments of originally longer chains.

Composition of Electron-Dense Particles. The nanometer-size electron-dense particles studied here are visible only in SEM-BSE, and no analytical method with sufficient resolution exists for this type of microscope to determine *in situ* the exact chemical composition of single crystals, except that they contain a heavy element. We suggest, however, that the following evidence very strongly, if not conclusively, indicates that the electron-dense particles are magnetite crystals: (*i*) The Fe-rich rim of carbonate globules, where the particles occur, contains large numbers of magnetite crystals of similar size range (2). (*ii*) After dissolution of the carbonate in 20% acetic acid, magnetite crystals are the only particulate structures left in the residue as identifiable in the transmission electron microscope (2) [with the exception of the rather rare iron sulfides (greigite and perhaps pyrrhotite), which have similar magnetic properties and are also known to be present in bacterial magnetosomes]. We repeated this test for confirmation of the results in ref. 2. (*iii*) The chains, as shown here, show a series of morphological features characteristic of magnetosome chains of bacteria that could not be explained by nonbiological processes. (*iv*) We used the two microanalytical techniques that come closest in resolution to our goal. Energy-dispersive x-ray spectrometry analyzes three-dimensional volumes, which we were able to reduce to 200 nm in diameter by working with a very low (5-kV) accelerating potential. Analyses at 24 points in the area of Fig. 4*A* (shown in Fig. 4*B*) showed the presence of excess Fe in some areas, compared with average ALH84001 orthopyroxene and rim carbonates, both of which have a narrow compositional range (2, 17). The iron level is highest in the area of dense conglomeration of particles (see details and spectra in *Appendix 2,* which is published as supplemental data on the PNAS web site, www.pnas.org). Auger electron spectroscopy, a method for surface compositional analysis, was used for the resin-embedded and polished specimen in Fig. 4*C*. Although the diameter of the incident beam was <60 nm, real analytical resolution was estimated as <400 nm, because of backscatter contribution. Fe/Mg and O/Mg ratios were measured at five points in the carbonate substrate without particles present (triangles) and at five points with short chains (squares). At these points, the Fe and O contents were elevated (Fig. 4*D*). On the basis of these considerations and analyses, we conclude that the electron-dense particles are identical with the magnetite (Fe_3O_4) crystals described by Thomas-Keprta *et al.* (2).

Discussion

Fossil magnetite crystals of magnetotactic bacteria have been described as ''magnetofossils'' (18), mostly identified by the morphology of single crystals. In a few cases, fragments of fossil chains (among them chains with strong but smooth bends) could be isolated from soft deep-sea sediments and studied by transmission electron microscopy (14). In this study we were able to visualize the *in situ* spatial orientation of magnetite crystals and chains inside a solid rock substrate.

The syngeneticity of these particles is evident because they are embedded in the carbonate globules, which quite certainly were

formed on Mars (1, 19, 20). Furthermore, Fig. 3*A* shows lobes of a carbonate globule containing magnetite chains (Fig. 3*E*) embedded in plagioclase glass and orthopyroxene.

The magnetite crystals in ALH84001 form chains similar to those in modern magnetotactic bacteria. This information should satisfy the last of the six criteria postulated (2) as evidence of biological origin. We also describe five additional criteria characteristic of biologically produced magnetite chains, which could not be present in abiotically formed chains of magnetite crystals (no such chains have ever been observed in nature). We suggest that these criteria have now been satisfied: *Uniform crystal size and shape within chains* is seen in Fig. 1 *G* and *H*, Fig. 1 *J* and *K*, and Fig. 4*A* (in the latter the crystals in the chain marked by an arrow are elongated and larger in diameter than those in the numerous chains of smaller and approximately isodiametric crystals), as well as in Fig. 3 *B–F*, which show chains of different sizes. Fig. 3 *E* and *F* (note different scales) show the difference between the largest, approximately isodiametric, and the smallest, elongated, crystals. No abiological process is known that would result in such sorting of crystals from a mixed pool of sizes and shapes. *Gaps between crystals* are best seen in Fig. 3*B*, although they are evident in all sufficiently resolved chains as dark lines between crystals. *Orientation of elongated crystals along the chain axis* is evident in Figs. 3*F* and 4*A* (arrow). *Halo around chains*, the possible remnant of a membrane, is visible in Fig. 1 *G–I*. *Flexibility of chains,* a character ascribable to the elastic property of the organic substance between but independent from the shape of the crystals, is evident in many of the small chains in Fig. 1 *G–I*, Fig. 1 *J–L*, and Fig. 3 *B–F*. We conclude that the chains of electron-opaque particles in ALH84001 are magnetofossils, as no other consistent explanation would account for these findings.

The ecological implications of the assumption that the magnetite chains in ALH84001 are of biological origin must be examined: Is it likely, on the basis of our knowledge of terrestrial magnetotactic bacteria, that such microorganisms were present in cracks of ALH84001? Numerous endolithic microorganisms exist in both terrestrial (21) and aquatic (22) habitats, yet it is very unlikely that magnetotactic bacteria were ever alive in ALH84001. All known endolithic microorganisms are sessile, attached to the surface; none is motile, understandable because swimming would be impossible in the microscopic spaces in rocks. Magnetotactic bacteria, with magnetosomes to serve as guides in the direction of swimming, are all motile. Furthermore, the non-Gaussian frequency distribution of the number of crystals in chains (Table 1) is incompatible with the variability of chain length in a living population. We suggest the following scenario: First, decomposed remains of dead magnetobacteria suspended in a carbonate-rich fluid penetrated fissures of ALH84001, already crushed by previous asteroid impact, perhaps after the second impact event (I2) postulated (23). Second, evaporation of the liquid led to the deposition of pancake-shaped carbonate globules, and magnetite crystals and chain fragments were deposited in the periphery of the carbonate discs, perhaps through the mechanism for ring deposition of particles dispersed in liquid drops (24).

Thanks are due to D. A. Bazylinski, J. L. Kirschvink, and J. W. Schopf for critical reading of the manuscript; to H. Jaksch and J. Greiser (LEO GmbH, Oberkochen, Germany) for help and cooperation in taking micrographs in Figs. 1 *A, B, D–L,* and 4*A*; to S. Douglass (Jet Propulsion Laboratory, Pasadena, CA) for Fig. 1*C*; to J. F. Almagro (Acerinox, Algeciras, Spain) for Figs. 3 *B* and *C* and 4*C*; to R. Bargallo, L. E. Bertani, L. Calvo-Barrio, A. Martinez, F. Pinto, and K. Riddle for support and technical help; and to A. B. Thistle for critical editing. This work was supported by National Aeronautics and Space Administration Grants NAG5/4921 and -9845 to E.I.F., Direcció General de Recerca de Generalitat de Catalunya Grant ACES98-15/1 to J.W., and Ministerio de Educación y Cultura Grant APC1998-0045 to C.A. and J.W.

1. McKay, D. S., Gibson, E. K., Jr., Thomas-Keprta, K. L., Vali, H., Romanek, C. S., Clemett, S. J., Chillier, X. D. F., Maechling, C. R. & Zare, R. N. (1996) *Science* **273,** 924–930.
2. Thomas-Keprta, K. L., Bazylinski, D. A., Kirschvink, J. L., Clemett, S. J., McKay, D. S., Wentworth, S. J., Vali, H., Gibson, E. K., Jr., & Romanek, C. S. (2000) *Geochim. Cosmochim. Acta* **64,** 4049–4081.
3. Friedmann, E. I., Wierzchos, J. & Ascaso, C. (1998) in *Workshop on the Issue of Martian Meteorites* (Lunar Planetary Institute, Houston, TX), Contribution 956, pp. 14–16.
4. Ascaso, C., Wierzchos, J. & de los Rios, A. (1995) *Bot. Acta* **108,** 474–481.
5. Joy, D. C. (1991) *Scanning Microsc.* **5,** 329–337.
6. Gorby, Y. A., Beveridge, T. J. & Blakemore, R. P. (1988) *J. Bacteriol.* **170,** 834–871.
7. Bazylinski, D. A. & Moskowitz, B. M. (1997) *Rev. Mineral.* **35,** 181–223.
8. Shcherbakov, V. P., Winklhofer, M., Hanzlik, M. & Petersen, N. (1997) *Eur. Biophys. J.* **26,** 319–326.
9. Butler, R. F. & Banerjee, S. K. (1975) *J. Geophys. Res.* **80,** 4049–4058.
10. Blakemore, R. P., Blakemore, N. A., Bazylinski, D. A. & Moench, T. T. (1989) in *Bergey's Manual of Systematic Bacteriology,* eds. Staley, J. T., Bryant, M. P., Pfennig, N. & Holt, J. G. (Williams & Wilkins, Baltimore), Vol. 3, pp. 1882–1889.
11. Frankel, R. B. & Bazylinski, D. A. (1994) *Hyperfine Interact.* **90,** 135–142.
12. Lowenstam, H. A. (1981) *Science* **211,** 1126–1131.
13. Kirschvink, J. L. (1982) *Earth Planet. Sci. Lett.* **59,** 388–392.
14. von Dobeneck, T., Petersen, N. & Vali, H. (1987) *Geowissenschaften in unserer Zeit* **5,** 27–35.
15. Mann, S. & Frankel, R. B. (1989) *in Biomineralization: Chemical and Biochemical Perspectives,* eds. Mann, S., Webb., J. & Williams, R. J. P. (VCH, New York), pp. 389–426.
16. Bazylinski, D. A., Garratt-Reed, A. J. & Frankel, R. B. (1994) *Microsc. Res. Tech.* **27,** 389–401.
17. Mittlefehldt, D. W. (1994) *Meteoritics* **29,** 214–221.
18. Chang, S.-B. R. & Kirschvink, L. M. (1989) *Annu. Rev. Earth Planet. Sci.* **17,** 169–195.
19. Romanek, C. S., Grady, M. M., Wright, I. P., Mittlefehldt, D. W., Socki, R. A., Pillinger, C. T. & Gibson, E. K., Jr. (1994) *Nature (London)* **372,** 655–657.
20. Borg, L. E., Connelly, J. N., Nyquist, L. E., Shih, C.-Y., Wiesmann, H. & Reese, Y. (1999) *Science* **286,** 90–93.
21. Friedmann, E. I. & Ocampo-Friedmann, R. (1984) in *Current Perspectives in Microbial Ecology*, eds. Klug, M. J. & Reddy, C. A. (Am. Soc. Microbiol., Washington, DC), pp. 177–185.
22. Golubic, S., Perkins, R. D. & Lukas, K. J. (1975) in *The Study of Trace Fossils*, ed. Frey, R.W. (Springer, New York), pp. 177–185.
23. Treiman, A. H. (1998) *Meteor. Planet. Sci.* **33,** 753–764.
24. Deegan, R. D., Bakajin, O., Dupont, T. F., Huber, G., Nagel, S. R. & Whitten, T. A. (1997) *Nature (London)* **389,** 827–829.